

Sensitive and Reversible Detection of Methanol and Water Vapor by In Situ Electrochemically Grown CuBTC MOFs on Interdigitated Electrodes

Sachdeva, Sumit; Venkatesh, Manjunath R.; Mansouri, Brahim El; Wei, Jia; Bossche, Andre; Kapteijn, Freek; Zhang, Guo Qi; Gascon, Jorge; de Smet, Louis C.P.M.; Sudhölter, Ernst

DOI

[10.1002/smll.201604150](https://doi.org/10.1002/smll.201604150)

Publication date

2017

Document Version

Final published version

Published in

Small

Citation (APA)

Sachdeva, S., Venkatesh, M. R., Mansouri, B. E., Wei, J., Bossche, A., Kapteijn, F., Zhang, G. Q., Gascon, J., de Smet, L. C. P. M., & Sudhölter, E. (2017). Sensitive and Reversible Detection of Methanol and Water Vapor by In Situ Electrochemically Grown CuBTC MOFs on Interdigitated Electrodes. *Small*, *13*(29), 160450-1-160450-6. Article 160450. <https://doi.org/10.1002/smll.201604150>

Important note

To cite this publication, please use the final published version (if applicable).
Please check the document version above.

Copyright

Other than for strictly personal use, it is not permitted to download, forward or distribute the text or part of it, without the consent of the author(s) and/or copyright holder(s), unless the work is under an open content license such as Creative Commons.

Takedown policy

Please contact us and provide details if you believe this document breaches copyrights.
We will remove access to the work immediately and investigate your claim.

Sensitive and Reversible Detection of Methanol and Water Vapor by In Situ Electrochemically Grown CuBTC MOFs on Interdigitated Electrodes

Sumit Sachdeva, Manjunath R. Venkatesh, Brahim El Mansouri, Jia Wei, Andre Bossche, Freek Kapteijn, Guo Qi Zhang, Jorge Gascon, Louis C. P. M. de Smet,* and Ernst J. R. Sudhölter

The in situ electrochemical growth of Cu benzene-1,3,5-tricarboxylate (CuBTC) metal–organic frameworks, as an affinity layer, directly on custom-fabricated Cu interdigitated electrodes (IDEs) is described, acting as a transducer. Crystalline 5–7 μm thick CuBTC layers are grown on IDEs consisting of 100 electrodes with a width and a gap of both 50 μm and a height of 6–8 μm. These capacitive sensors are exposed to methanol and water vapor at 30 °C. The affinities show to be completely reversible with higher affinity toward water compared to methanol. For exposure to 1000 ppm methanol, a fast response is observed with a capacitance change of 5.57 pF at equilibrium. The capacitance increases in time followed diffusion-controlled kinetics ($k = 2.9 \text{ mmol s}^{-0.5} \text{ g}^{-1} \text{ CuBTC}$). The observed capacitance change with methanol concentration follows a Langmuir adsorption isotherm, with a value for the equilibrium affinity $K_e = 174.8 \text{ bar}^{-1}$. A volume fraction $f_{\text{MeOH}} = 0.038$ is occupied upon exposure to 1000 ppm of methanol. The thin CuBTC affinity layer on the Cu-IDEs shows fast, reversible, and sensitive responses to methanol and water vapor, enabling quantitative detection in the range of 100–8000 ppm.

S. Sachdeva, Prof. F. Kapteijn, Prof. J. Gascon,
Dr. L. C. P. M. de Smet, Prof. E. J. R. Sudhölter
Department of Chemical Engineering
Delft University of Technology
Van der Maasweg 9, 2629 HZ, Delft, The Netherlands
E-mail: louis.desmet@wur.nl

M. R. Venkatesh, Prof. G. Q. Zhang
Beijing Research Centre
Delft University of Technology
Mekelweg 4, 2628 CD, Delft, The Netherlands
B. E. Mansouri, Dr. J. Wei, Dr. A. Bossche, Prof. G. Q. Zhang
Department of Microelectronics
Delft University of Technology
Mekelweg 4, 2628 CD, Delft, The Netherlands

Dr. L. C. P. M. de Smet
Laboratory of Organic Chemistry
Wageningen University & Research
Stippeneng 4, 6708 WE, Wageningen, The Netherlands



Recent advances in the microelectronics industry have resulted in the development of miniaturized transduction devices for accurate, real-time detection of various analytes. Such systems require, in addition, affinity layers for the introduction of sensitive, selective, and reversible interactions with the analytes to be detected.^[1] While most of the commercially available sensors utilize metal-oxides as affinity layers, there is interest for extending the range of affinity materials to reduce cross-sensitivity and to lower energy consumption.^[2] Recent studies have focused on utilizing metal–organic frameworks (MOFs) as affinity layer materials, because of their high porosity, selective gas adsorption properties, and tunability.^[3] MOFs belong to the class of hybrid materials and are composed of coordinatively linked metal ions or clusters via organic ligands to form porous crystalline frameworks.^[3b,4] Hitherto, most of the sensing studies with MOFs were carried out using the material as a bulk powder, i.e., by monitoring the change of luminescence properties

DOI: 10.1002/sml.201604150

upon analyte binding.^[3a,5] Only a few studies have appeared on postsynthetically deposited MOFs on a transducer surface, able to transform the interactions with the analyte into changes of conductivity or dielectric properties.^[6] The layer-by-layer deposition method has also been used to make thin films of MOFs on the surface of transducers.^[7] While all these multiple-step approaches illustrate well the attractiveness of using MOFs as selective affinity layers for sensor devices, their further applicability will benefit from developments that shorten the fabrication process of the MOF coatings.^[8]

An interesting approach to grow MOF films directly on metal (transducer) surfaces in a fast and controllable way makes use of anodic dissolution of the metal ions in the presence of the organic linkers.^[9] Such an electrochemical deposition procedure can be easily integrated with semiconductor processing techniques.^[10] Recently, the ability to grow Cu-MOFs as uniform films on flat Cu electrodes by applying cyclic current pulses is shown.^[11] The electrochemical growth of Cu-MOFs on interdigitated Cu electrodes as sensors and their ability to detect methanol and water vapor at room temperature is demonstrated. These analytes were chosen as the model candidates to study the feasibility of this MOF-transducer integration technique due to their known affinity toward CuBTC.^[12] The interdigitated electrode (IDE) structure allows capacitive detection^[13] of the affinity process. IDEs can easily be fabricated, are compatible with CMOS technology and are able to operate at room temperature allowing for a low power consumption.^[13a,14]

The IDEs were fabricated on p-type silicon substrates by photolithography using two different procedures with either positive or negative photoresist to pattern the IDE structures (**Figure 1** and Figure S1 and Section S1.1 (Supporting

information)). Next, Cu was electroplated utilizing a presputtered 300 nm Cu seed layer as cathode to obtain the planar electrodes with varying widths (W) and gaps (G) ranging from 5 to 50 μm (Figure 1i–iii). For this study, IDEs with $W = G = 50 \mu\text{m}$ and a number of electrodes (N) of 100 are used, to ensure a good coverage of the MOF and to prevent electrical shortcuts which might arise at smaller G . Since the total capacitance is a linear function of N , it was set at the indicated value to enhance the overall sensitivity. The height of the produced Cu electrodes was 6–8 μm , as determined by cross-sectional scanning electron microscopy (SEM, Figure 1iv) and by Dektak profilometry (Figure S2, Supporting Information). The spatial wavelength^[15] (λ) of the IDE device is defined by:

$$\lambda = 2(W + G) \quad (1)$$

The sensitivity of the IDE transducer to detect changes in the capacitance of the affinity layer increases with a smaller value of λ . Theoretical calculations of the electric field properties and the capacitance of our IDE structures making use of COMSOL Multiphysics^[16] for a configuration of two half electrodes (half spatial wavelength (λ)) were performed. The total capacitance was estimated by multiplying the resulting modeled capacitance with $(N - 1) = 99$, to yield a $(N - 1) \times C_{\text{electrode}}$. The width (W) and gap (G) of the IDE structure were both set to 50 μm in COMSOL^[16] and the height of the electrodes was set to 6 and 3 μm , to simulate the situation before and after the MOF growth process, respectively (Section S1.3, Supporting Information).

From Figure 1v, it can be seen that the field strength remains strongest near the surface of the electrodes. About 75% of the field lines are found at a distance of $z < 40 \mu\text{m}$,

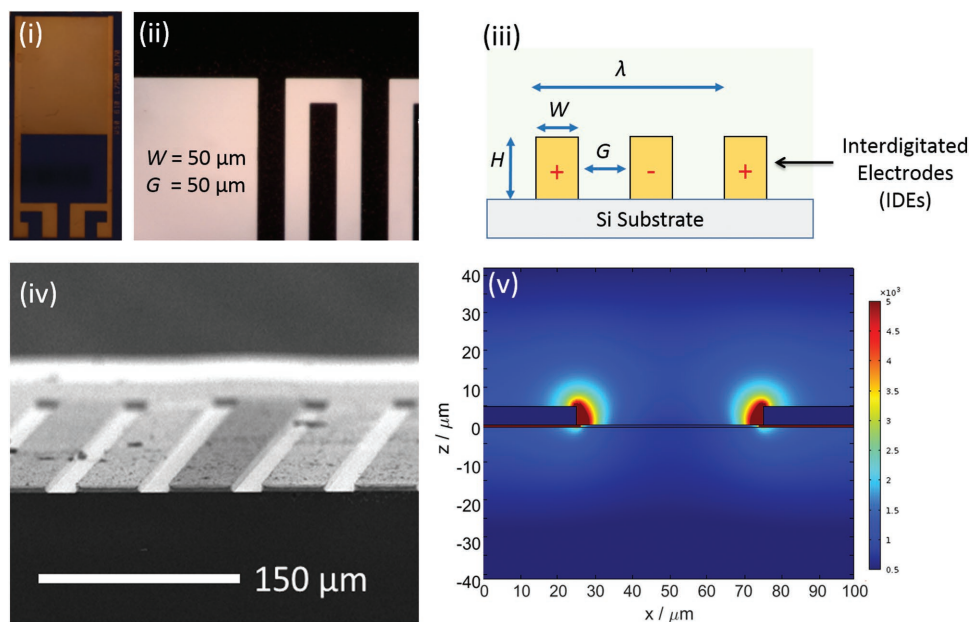


Figure 1. Fabricated devices with interdigitated electrodes (IDEs). i) Optical image of the fabricated IDE with four-bond pads in the end for external connections and ii) optical image of a region of the IDEs with electrodes (black region) with width (W) and gap (G) of each 50 μm . iii) Schematic of the device illustrating the dimensions (width (W), gap (G), and height (H) of the electrodes) and spatial wavelength (λ) of the device. iv) SEM image of the IDEs width of 50 μm and gap of 20 μm captured at 6° angle view and v) figure indicating the distribution and electrical field strength (V m^{-1}) calculated across x and z dimensions. Color map indicates a distribution from the weakest (in blue) to the strongest (in red) field strength (V m^{-1}).

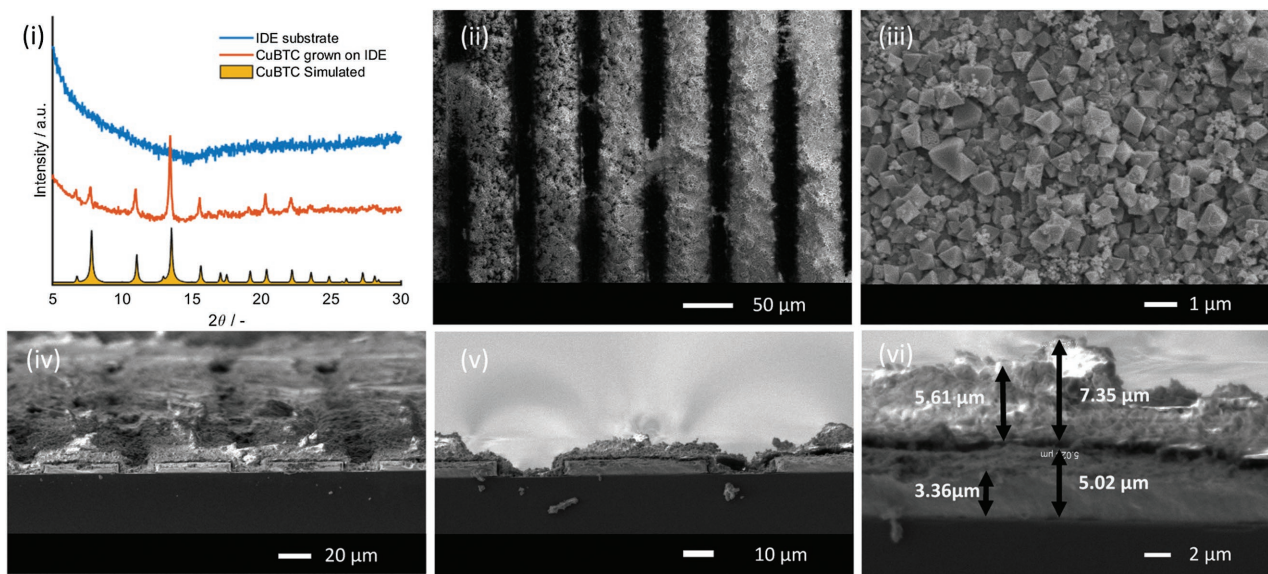


Figure 2. i) Comparison of the XRD pattern for the IDEs with (red) and without (blue) CuBTC layer with the simulated pattern of CuBTC. ii,iii) SEM images of CuBTC grown over the electrodes. iv–vi) Cross-sectional SEM of a coated IDE.

as measured perpendicular to the electrode surface. Near the edges of the electrodes (i.e., region between $x = 0$ – $25 \mu\text{m}$ and $x = 75$ – $100 \mu\text{m}$ in Figure 1v; red colored) the maximal electrical field strength was found. A capacitance of 132 pF was calculated for IDE with $W = G = 50 \mu\text{m}$ and $N = 100$. Experimentally, the capacitance of the IDE was $3940.0 \pm 0.1 \text{ pF}$ at 20 kHz (Figure S3, Supporting Information). The observed larger capacitance compared to the calculated capacitance is due to the parasitic contributions from the substrate and the wire bonding ($\approx 3000 \text{ pF}$; see Section S2 in the Supporting Information).

The Cu IDEs were used to electrochemically grow thin films of the well-known CuBTC MOF.^[17] It consists of a Cu paddlewheel framework formed from two Cu ions coordinated with four tridentate benzene-1,3,5-tricarboxylate (BTC) ligands (Figure S4, Supporting information).^[17a] CuBTC has affinity for small-size gases such as NH_3 , CO , NO_2 , NO , H_2S , I_2 , ClCN , and volatile organic components such as methanol and ethanol, making it a potential candidate for application as affinity layer on our IDEs.^[18] CuBTC was grown electrochemically on the Cu IDE structures with a Cu counter-electrode (cathode) in a 10 mL electrochemical cell containing a H_3BTC solution in 96 vol% ethanol (Section S1.2, Supporting Information). Cyclic pulses of the current (6 mA for 5 s followed by no current for 5 s) were applied for 5 min.^[11a] This resulted in the deposition of crystalline materials on the IDE structure. By X-ray diffraction (XRD), the formation of CuBTC was confirmed (Figure 2i).^[17a,19] The crystalline layer was uniformly grown and showed a thickness of 5–7 μm as deduced from SEM images (Figure 2 and Figure S5 (Supporting Information)). Cracks in the CuBTC layers were observed and also some crystal detachment if the pulses were applied during a longer time period (7.5 min). This is most likely due to induced mechanical stress by the partial dissolution of the copper finger-electrodes and the concomitant formation of CuBTC^[9b] (Figure S6, Supporting Information). The thickness of the IDE electrodes was reduced from

6–8 to 3–5 μm (Figure 2vi and Figure S2 (Supporting information)). N_2 and CO_2 adsorption studies on CuBTC deposited over Cu-Mesh confirmed the porosity of the deposited layer (Figure S7, Supporting information). Due to this electrochemical deposition process of CuBTC ($\epsilon_r = 1.7$),^[20] the device configuration is changed (Figure S8, Supporting Information). The presence of voids in the layer and noncoated region between electrodes is represented as a capacitance (C_{air}) in series with the capacitance introduced by the MOF layer (C_{MOF}) as indicated by Figure S8b (Supporting information). This series capacitance affects the sensitivity of the device but presence of CuBTC layer should enhance the adsorption. The deposition resulted in a slight decrease of the calculated capacitance from ≈ 132 to $\approx 122 \text{ pF}$ as a combined result of reduction in electrode thickness and growth of a higher dielectric layer (Figure S9, Supporting Information).

These CuBTC-modified IDEs were exposed to different concentrations of methanol and water vapor present in a nitrogen carrier gas at 30 °C in a custom-built gas mixing and sensing equipment system described previously.^[6c] The capacitance changes were determined by using impedance spectroscopy at a constant frequency of 20 kHz. In Figure 3i, a capacitive response of 5–25 pF is shown upon the exposure to 1000–8000 ppm of methanol at a constant flow rate of 200 mL min^{-1} , in contrast to the unmodified IDE that showed no response. The response of the modified device to methanol vapor was completely reversible. The desorption time is longer than the adsorption time, reflecting the so-called “favorable” methanol isotherm.

The capacitive response started a few seconds after applying the methanol and reached an equilibration value in 120–150 s (Figure 3ii). Such response is comparable with the metal-oxide based methanol sensors^[21] and clearly reflects the presence of the thin CuBTC layer with its high porosity (having a (Brunauer–Emmett–Teller)BET surface area of $\approx 1300 \text{ m}^2 \text{ g}^{-1}$ and a pore volume of $\approx 0.73 \text{ cm}^3 \text{ g}^{-1}$).^[12] By contrast, a coating of amino-MIL-53(Al) MOF blended

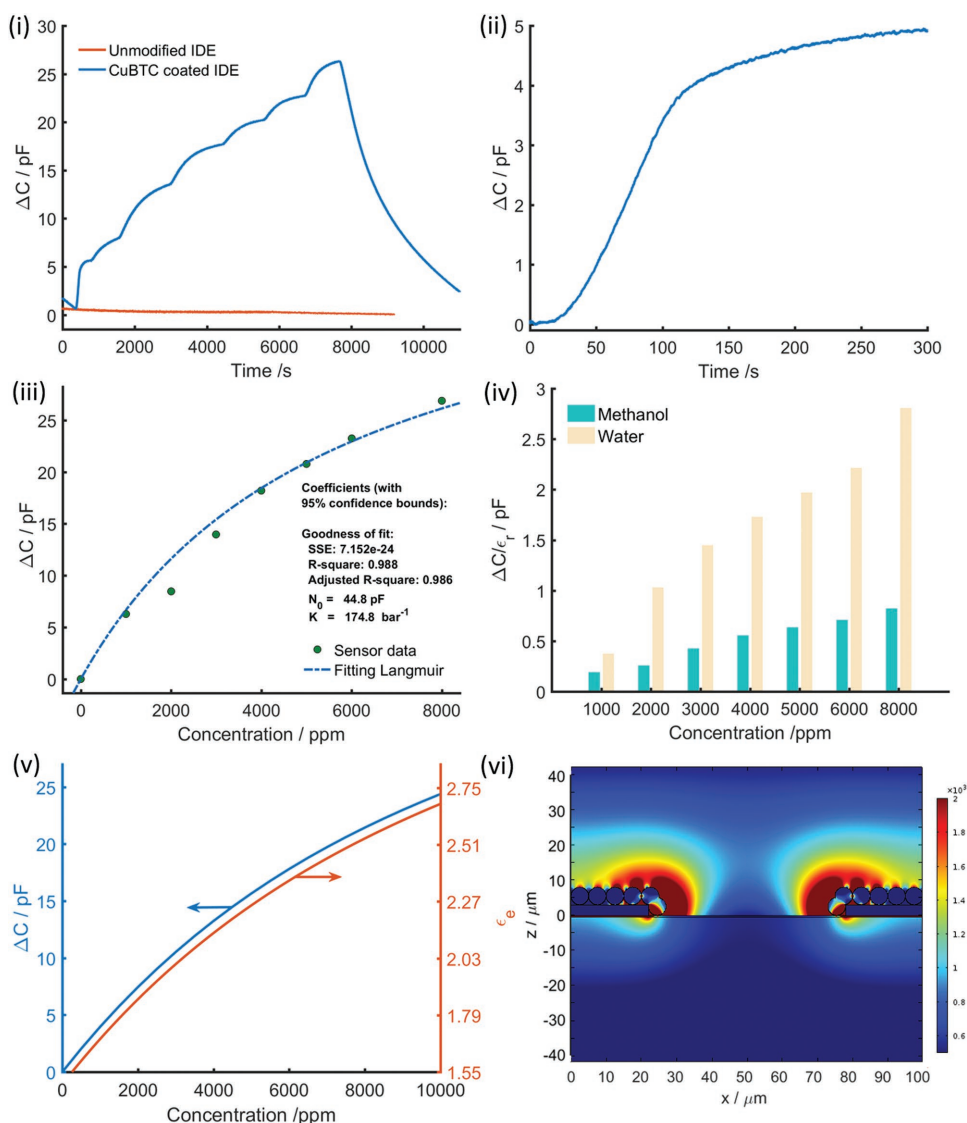


Figure 3. i) Capacitive response of unmodified IDE (red) and CuBTC-coated IDE (blue) toward methanol. ii) Capacitive response versus time of CuBTC-coated IDE toward 1000 ppm of methanol vapor. iii) Quantitative behavior of the sensor device toward methanol vapor and the Langmuir model fit. iv) Comparison between the response toward methanol and water vapor normalized with respect to the dielectric constants of analyte. v) Estimated dielectric constant (red) and capacitive change (blue) of these devices with methanol concentration as deduced by finite element analysis. vi) Simulated distribution of the electric field strength, $|E|$ over the IDE geometry. Color map indicates a distribution from the weakest (blue) to the strongest (red) field strength (V m^{-1}).

in a Matrimid polymeric matrix, shows a ≈ 12 times slower response.^[6c] This slower response is the result of the presence of the polymer, which acts as a diffusion barrier.^[6c]

Next, this capacitive increase in time for the situation where 1000 ppm of methanol vapor was applied, was further analyzed to understand the role of pore diffusion in the methanol sensing. At these analyte concentrations, the methanol adsorption takes place mostly at the open-metal sites of CuBTC framework^[12] which have a cage diameter of 9 Å with a pore window between 3.5 and 4.6 Å. With a kinetic diameter of 3.6 Å, diffusion of methanol within the CuBTC framework can significantly affect the adsorption process and hence the sensor response. Diffusion studies on CuBTC with gases such as CO_2 (kinetic diameter 3.3 Å) clearly indicate the role of intraparticle diffusion.^[22] Such intraparticle diffusion plays a dominant role in the adsorption processes, if the

uptake and hence the sensor response is directly proportional with the square root of the time ($t^{0.5}$) as described below:^[23] (Equation (2); Section 5, Supporting information)

$$\Delta C = k_p t^{0.5} + I \quad (2)$$

where ΔC is the change in capacitance at time t , k_p is the rate constant, and I is the intercept representing the boundary layer effects. Figure S10 (Supporting information) shows that the relation between ΔC and $t^{0.5}$ can be divided into three regimes. The first section shows a very small increase in capacitance ($t^{0.5} < 4 \text{ s}^{0.5}$) and can be accounted for the equilibration of the measurement chamber due to the presence of large dead-volume (400–450 mL). It is followed by the linear regime of the response indicating the dominance of the intraparticle diffusion in the adsorption process. The rate

constant (k_p) for this diffusion-controlled process was determined to be $0.648 \text{ pF s}^{-0.5}$ with a R^2 value of 0.9958. The third section represents the equilibrium stage ($t^{0.5} > 9 \text{ s}^{0.5}$) where a decrease in the concentration gradient slows down the diffusion process.

The capacitance response, (ΔC), in the measured methanol concentration range was further related to the concentration of methanol in the CuBTC affinity layer near the transducer by applying a Langmuir isotherm model as indicated in Figure 3iii and described by Equation (3):

$$\frac{\Delta C}{C_s} = \frac{K_e c_m}{1 + K_e c_m} = \frac{q}{q_s} = \theta \quad (3)$$

where C_s , K_e , c_m , and q_s indicate the saturation capacitance, affinity constant, concentration of methanol in the measurement chamber, and saturated amount of adsorbed methanol, respectively. K_e and C_s were found to be 174.8 bar^{-1} and $\approx 44.8 \text{ pF}$, respectively, as determined by nonlinear least square fitting of Equation S5 (Supporting Information) to the experimental sensor response. Even though C_s indicates that the adsorption capacity is still far from saturation, extrapolation to higher concentration has to be done carefully as multiple-site adsorption and pore filling in CuBTC can result in deviations from Langmuir behavior.^[12] Based on these parameters, the amount of adsorbed methanol for applying a 1000 ppm concentration was estimated to be $\approx 2.9 \text{ mmol g}^{-1}$ of CuBTC (corresponding to a 5.57 pF capacitive change and $q_s = \approx 0.02 \text{ mol g}^{-1}$).^[24] These estimated adsorbed amounts (from 2.9 to 11.6 mmol g^{-1}) for the applied methanol concentration range (1000–8000 ppm) were well in correspondence with the literature.^[12] Utilizing the amount of adsorbed methanol, the diffusion rate constant was also recalculated as $0.29 \text{ mmol s}^{-0.5} \text{ g}^{-1} \text{ CuBTC}$. Furthermore, changes in the volume fraction (f) of methanol inside the pores of CuBTC were also calculated on exposure to different concentrations of methanol vapor with the assumption of a Langmuir behavior of adsorption (Section S6 and Figure S11, Supporting information). For 1000 ppm of methanol in N_2 , f_{MeOH} was calculated to be 0.038.

With an accuracy of our equipment (HP 4284A LCR meter) in the fF range, the sensitivity of the devices is clearly indicated by changes of $5 \text{ pF}/1000 \text{ ppm}$ of methanol. Our CuBTC-modified IDEs were also exposed to different concentrations of water vapor and the results were compared with the responses observed to methanol (Figure 3iv). The responses were therefore corrected for the differences of dielectric constants of methanol and water by dividing the observed capacitance change by the respective dielectric constants ($\epsilon_{r, \text{methanol}} = 32.7$, $\epsilon_{r, \text{water}} = 78$). Clearly, the affinity of the CuBTC toward water vapor is much stronger than the observed affinity to methanol. This observation confirms earlier studies.^[18a] For lower methanol concentrations ($\approx 100 \text{ ppm}$) similar results related to reversibility and reproducibility were found (Figures S12–S15 and Section S7, Supporting information).

The methanol adsorption by the CuBTC framework also changes the effective local dielectric constant (ϵ_e). This ϵ_e was approximated utilizing the Bruggeman effective medium

approximation^[25] which is based on changes in the volumetric fraction (f) (Section S6, Supporting information). The relative static dielectric constant of CuBTC^[20a] (in vacuum) was assumed to be $\epsilon_r = 1.7$. It can be seen in Figure 3v that the calculated ϵ_e roughly increases from ≈ 1.5 to ≈ 2.7 on exposure from 0 to 8000 ppm of methanol ($\epsilon_r = 32.7$). The calculated capacitance (by finite element modeling) for these dielectric constant changes are in line with the measured capacitance changes, confirming the role of changes in local polarity on the adsorption of polar molecules like methanol. Finally, the simulated electric field strength of these MOF-modified electrodes indicated a slight decrease with this increase of ϵ_r to 2.7 (Figure 3vi and Figures S16 and S17 (Supporting information)).

In summary, the feasibility of in situ electrochemically grown CuBTC MOFs on Cu IDEs as sensor devices is successfully demonstrated. To best of our knowledge, this is the first study for such MOF-transducer integration. These devices show a fast response (120–150 s to saturation), are sensitive and have reversible sensing properties useful for the quantitative detection of methanol and water vapor in the 100–8000 ppm range. The time-dependent responses were successfully simulated by the diffusion-controlled kinetics. Equilibrium capacitive responses also followed the Langmuir adsorption model with an affinity constant of 174 bar^{-1} for methanol concentrations up to 8000 ppm. Comparative sensing studies with methanol and water indicated higher sensitivity toward water due to its stronger affinity to the CuBTC. Theoretical estimations of the local dielectric constants by application of the Bruggeman approximation, indicated that on the exposure to different methanol vapor concentrations (0–8000 ppm), the relative dielectric constant of partially filled CuBTC increases from ≈ 1.5 to ≈ 2.7 as a result of the uptake of methanol. The calculated capacitance changes correlate well with the experimentally observed data, supporting our applied methods. In conclusion, CuBTC MOFs can be formed in situ electrochemically on microstructured copper IDEs in a fast and easy way. These devices act as fast, reversible and sensitive sensors for the quantitative detection of methanol and water vapor in the range of 100–8000 ppm.

Supporting Information

Supporting Information is available from the Wiley Online Library or from the author.

Acknowledgements

S.S. and M.R.V. contributed equally to the work. S.S., F.K., J.G., L.C.P.M.d.S., and E.J.R.S. acknowledge NanoNextNL, a micro and nanotechnology consortium of the Government of The Netherlands and 130 partners, for financial support. Anping Cao (TU Delft) is thanked for help with cross-sectional SEM measurements.

Conflict of Interest

The authors declare no conflict of interest.

- [1] a) C. Hagleitner, A. Hierlemann, D. Lange, A. Kummer, N. Kerness, O. Brand, H. Balthes, *Nature* **2001**, *414*, 293; b) X.-J. Huang, Y.-K. Choi, *Sens. Actuators, B* **2007**, *122*, 659.
- [2] a) D. R. Miller, S. A. Akbar, P. A. Morris, *Sens. Actuators, B* **2014**, *204*, 250; b) Y.-F. Sun, S.-B. Liu, F.-L. Meng, J.-Y. Liu, Z. Jin, L.-T. Kong, J.-H. Liu, *Sensors* **2012**, *12*, 2610.
- [3] a) F.-Y. Yi, D. Chen, M.-K. Wu, L. Han, H.-L. Jiang, *ChemPlusChem* **2016**, *81*, 675; b) D. J. Wales, J. Grand, V. P. Ting, R. D. Burke, K. J. Edler, C. R. Bowen, S. Mintova, A. D. Burrows, *Chem. Soc. Rev.* **2015**, *44*, 4290; c) I. Stassen, B. Bueken, H. Reinsch, J. F. M. Oudenhoven, D. Wouters, J. Hajek, V. Van Speybroeck, N. Stock, P. M. Vereecken, R. Van Schaijk, D. De Vos, R. Ameloot, *Chem. Sci.* **2016**, *7*, 5827.
- [4] A. U. Czaja, N. Trukhan, U. Muller, *Chem. Soc. Rev.* **2009**, *38*, 1284.
- [5] Z. Hu, B. J. Deibert, J. Li, *Chem. Soc. Rev.* **2014**, *43*, 5815.
- [6] a) M. G. Campbell, D. Sheberla, S. F. Liu, T. M. Swager, M. Dinca, *Angew. Chem.* **2015**, *127*, 4423; b) S. Achmann, G. Hagen, J. Kita, I. Malkowsky, C. Kiener, R. Moos, *Sensors* **2009**, *9*, 1574; c) S. Sachdeva, D. Soccol, D. J. Gravesteijn, F. Kapteijn, E. J. R. Sudhölter, J. Gascon, L. C. P. M. de Smet, *ACS Sens.* **2016**, *1*, 1188.
- [7] a) H. Gliemann, C. Wöll, *Mater. Today* **2012**, *15*, 110; b) L. Heinke, M. Tu, S. Wannapaiboon, R. A. Fischer, C. Wöll, *Microporous Mesoporous Mater.* **2015**, *216*, 200; c) C. Sapsanis, H. Omran, V. Chernikova, O. Shekhah, Y. Belmabkhout, U. Buttner, M. Eddaoudi, K. Salama, *Sensors* **2015**, *15*, 18153.
- [8] a) H. K. Arslan, O. Shekhah, J. Wohlgemuth, M. Franzreb, R. A. Fischer, C. Wöll, *Adv. Funct. Mater.* **2011**, *21*, 4228; b) I. Stassen, M. Styles, G. Greci, H. V. Gorp, W. Vanderlinden, S. D. Feyter, P. Falcaro, D. D. Vos, P. Vereecken, R. Ameloot, *Nat. Mater.* **2016**, *15*, 304.
- [9] a) W.-J. Li, M. Tu, R. Cao, R. A. Fischer, *J. Mater. Chem. A* **2016**, *4*, 12356; b) N. Campagnol, T. R. C. Van Assche, M. Li, L. Stappers, M. Dinca, J. F. M. Denayer, K. Binnemans, D. E. De Vos, J. Fransaer, *J. Mater. Chem. A* **2016**, *4*, 3914; c) I. Stassen, M. Styles, T. Van Assche, N. Campagnol, J. Fransaer, J. Denayer, J.-C. Tan, P. Falcaro, D. De Vos, R. Ameloot, *Chem. Mater.* **2015**, *27*, 1801; d) B. Van de Voorde, R. Ameloot, I. Stassen, M. Everaert, D. De Vos, J.-C. Tan, *J. Mater. Chem. C* **2013**, *1*, 7716.
- [10] a) M. Beidaghi, Y. Gogotsi, *Energy Environ. Sci.* **2014**, *7*, 867; b) G. Oskam, J. G. Long, A. Natarajan, P. C. Searson, *J. Phys. D: Appl. Phys.* **1998**, *31*, 1927.
- [11] a) S. Sachdeva, A. Pustovarenko, E. J. R. Sudhölter, F. Kapteijn, L. C. P. M. de Smet, J. Gascon, *CrystEngComm* **2016**, *18*, 4018; b) A. Martinez Joaristi, J. Juan-Alcañiz, P. Serra-Crespo, F. Kapteijn, J. Gascon, *Cryst. Growth Des.* **2012**, *12*, 3489.
- [12] T. R. C. Van Assche, T. Duerinck, J. J. Gutiérrez Sevillano, S. Calero, G. V. Baron, J. F. M. Denayer, *J. Phys. Chem. C* **2013**, *117*, 18100.
- [13] a) N. F. Sheppard, R. C. Tucker, C. Wu, *Anal. Chem.* **1993**, *65*, 1199; b) U. Altenberend, F. Molina-Lopez, A. Oprea, D. Briand, N. Bârsan, N. F. De Rooij, U. Weimar, *Sens. Actuators, B* **2013**, *187*, 280.
- [14] Y. Lu, J. Li, J. Han, H. T. Ng, C. Binder, C. Partridge, M. Meyyappan, *Chem. Phys. Lett.* **2004**, *391*, 344.
- [15] a) N. Igreja, C. J. Dias, *Sens. Actuators, A* **2004**, *112*, 291; b) R. Igreja, C. J. Dias, *Sens. Actuators, B* **2006**, *115*, 69.
- [16] P. Oikonomou, A. Salapatias, K. Manoli, K. Misiakos, D. Goustouridis, E. Valamontes, M. Sanopoulou, I. Raptis, G. P. Patsis, *Procedia Eng.* **2011**, *25*, 423.
- [17] a) S. S.-Y. Chui, S. M.-F. Lo, J. P. H. Charmant, A. G. Orpen, I. D. Williams, *Science* **1999**, *283*, 1148; b) T. R. C. Van Assche, G. Desmet, R. Ameloot, D. E. De Vos, H. Terryn, J. F. M. Denayer, *Microporous Mesoporous Mater.* **2012**, *158*, 209.
- [18] a) S. Calero, P. Gómez-Álvarez, *J. Phys. Chem. C* **2015**, *119*, 467; b) P. Davydovskaya, A. Ranft, B. V. Lotsch, R. Pohle, *Anal. Chem.* **2014**, *86*, 6948; c) M. S. Hosseini, S. Zeinali, M. H. Sheikhi, *Sens. Actuators, B* **2016**, *230*, 9; d) J. B. DeCoste, G. W. Peterson, *Chem. Rev.* **2014**, *114*, 5695.
- [19] A. Vishnyakov, P. I. Ravikovitch, A. V. Neimark, M. Bülow, Q. M. Wang, *Nano Lett.* **2003**, *3*, 713.
- [20] a) K. Zagorodniy, G. Seifert, H. Hermann, *Appl. Phys. Lett.* **2010**, *97*, 251905; b) E. Redel, Z. Wang, S. Walheim, J. Liu, H. Gliemann, C. Wöll, *Appl. Phys. Lett.* **2013**, *103*, 091903.
- [21] P. P. Sahay, R. K. Nath, *Sens. Actuators, B* **2008**, *134*, 654.
- [22] T. M. Tovar, J. Zhao, W. T. Nunn, H. F. Barton, G. W. Peterson, G. N. Parsons, M. D. LeVan, *J. Am. Chem. Soc.* **2016**, *138*, 11449.
- [23] a) R. Subramanian, V. Lakshminarayanan, *Electrochim. Acta* **2000**, *45*, 4501; b) F.-C. Wu, R.-L. Tseng, R.-S. Juang, *Chem. Eng. J.* **2009**, *153*, 1.
- [24] Y. Wu, H. Chen, J. Xiao, D. Liu, Z. Liu, Y. Qian, H. Xi, *ACS Appl. Mater. Interfaces* **2015**, *7*, 26930.
- [25] K. Lazarova, B. Georgieva, M. Spasova, T. Babeva, *J. Phys.: Conf. Ser.* **2014**, *558*, 012042.

Received: December 15, 2016
Revised: April 10, 2017
Published online: June 8, 2017